


## Article

# Study on the Method of Vineyard Information Extraction Based on Spectral and Texture Features of GF-6 Satellite Imagery

Xuemei Han <sup>1,2,3</sup>, Huichun Ye <sup>2,3,4,\*</sup> , Yue Zhang <sup>2,3,5</sup>, Chaojia Nie <sup>2,3</sup> and Fu Wen <sup>5</sup>

<sup>1</sup> College of Geology and Mining Engineering, Xinjiang University, Urumqi 830047, China; 107552204671@stu.xju.edu.cn

<sup>2</sup> International Research Center of Big Data for Sustainable Development Goals, Beijing 100094, China; zhangyue0961@link.tyut.edu.cn (Y.Z.); niecj@aircas.ac.cn (C.N.)

<sup>3</sup> Key Laboratory of Digital Earth Science, Aerospace Information Research Institute, Chinese Academy of Sciences, Beijing 100094, China

<sup>4</sup> Lab of Big Earth Data and Sustainable Development Goal (BASL), Kashi Aerospace Information Research Institute, Kashgar 844000, China

<sup>5</sup> College of Water Resources Science and Engineering, Taiyuan University of Technology, Taiyuan 030024, China; wenfu0847@link.tyut.edu.cn

\* Correspondence: yehc@aircas.ac.cn

**Abstract:** Accurately identifying the distribution of vineyard cultivation is of great significance for the development of the grape industry and the optimization of planting structures. Traditional remote sensing techniques for vineyard identification primarily depend on machine learning algorithms based on spectral features. However, the spectral reflectance similarities between grapevines and other orchard vegetation lead to persistent misclassification and omission errors across various machine learning algorithms. As a perennial vine plant, grapes are cultivated using trellis systems, displaying regular row spacing and distinctive strip-like texture patterns in high-resolution satellite imagery. This study selected the main oasis area of Turpan City in Xinjiang, China, as the research area. First, this study extracted both spectral and texture features based on GF-6 satellite imagery, subsequently employing the Boruta algorithm to discern the relative significance of these remote sensing features. Then, this study constructed vineyard information extraction models by integrating spectral and texture features, using machine learning algorithms including Naive Bayes (NB), Support Vector Machines (SVMs), and Random Forests (RFs). The efficacy of various machine learning algorithms and remote sensing features in extracting vineyard information was subsequently evaluated and compared. The results indicate that three spectral features and five texture features under a  $7 \times 7$  window have significant sensitivity to vineyard recognition. These spectral features include the Normalized Difference Vegetation Index (NDVI), Enhanced Vegetation Index (EVI), and Normalized Difference Water Index (NDWI), while texture features include contrast statistics in the near-infrared band (B4\_CO) and the variance statistic, contrast statistic, heterogeneity statistic, and correlation statistic derived from NDVI images (NDVI\_VA, NDVI\_CO, NDVI\_DI, and NDVI\_COR). The RF algorithm significantly outperforms both the NB and SVM models in extracting vineyard information, boasting an impressive accuracy of 93.89% and a Kappa coefficient of 0.89. This marks a 12.25% increase in accuracy and a 0.11 increment in the Kappa coefficient over the NB model, as well as an 8.02% enhancement in accuracy and a 0.06 rise in the Kappa coefficient compared to the SVM model. Moreover, the RF model, which amalgamates spectral and texture features, exhibits a notable 13.59% increase in accuracy versus the spectral-only model and a 14.92% improvement over the texture-only model. This underscores the efficacy of the RF model in harnessing the spectral and textural attributes of GF-6 imagery for the precise extraction of vineyard data, offering valuable theoretical and methodological insights for future vineyard identification and information retrieval efforts.

**Keywords:** remote sensing features; machine learning; Boruta algorithm; orchard extraction; feature selection



**Citation:** Han, X.; Ye, H.; Zhang, Y.; Nie, C.; Wen, F. Study on the Method of Vineyard Information Extraction Based on Spectral and Texture Features of GF-6 Satellite Imagery. *Agronomy* **2024**, *14*, 2542. <https://doi.org/10.3390/agronomy14112542>

Academic Editors: Yanbo Huang, Xin Zhang and Chandan Kumar

Received: 30 September 2024

Revised: 25 October 2024

Accepted: 26 October 2024

Published: 28 October 2024



**Copyright:** © 2024 by the authors. Licensee MDPI, Basel, Switzerland. This article is an open access article distributed under the terms and conditions of the Creative Commons Attribution (CC BY) license (<https://creativecommons.org/licenses/by/4.0/>).

## 1. Introduction

China is a major producer of grapes, accounting for 46% of the global total grape production as of 2022, and consistently holds the top position worldwide. Turpan City in the Xinjiang Uygur Autonomous Region accounts for 21% of China's grape production and 52% of Xinjiang's total production [1]. Accurately understanding the distribution of grape cultivation is crucial for promoting the development of the grape industry and optimizing planting structures [2–4]. However, the complexity of vineyard planting structures, the variation in sizes, and the extended growth cycles present challenges for effectively monitoring and managing the cultivated areas [5,6]. Traditional manual survey methods were inefficient and costly, while remote sensing technology, with its advantages of objectivity, timeliness, and large-area coverage, was widely applied in estimating vineyard cultivation areas and extracting planting regions [7,8]. The acquisition of remote sensing information for vineyards primarily relies on technologies such as satellite remote sensing and UAV (unmanned aerial vehicle) remote sensing. Compared to UAV remote sensing, satellite remote sensing can cover a much larger monitoring area and demonstrates greater stability when dealing with classification issues between the canopy and other objects, such as canopy shadow projections or the background between vineyard rows [9]. Additionally, the larger field of view and relatively lower resolution of satellite imagery help reduce classification confusion caused by shadows and background interference that often occur in high-resolution images, making it uniquely advantageous for large-scale vineyard management [9–11].

High-resolution satellite remote sensing imagery is highly valued for its richness of information. Since the launch of the High-Resolution Earth Observation System Major Project in China, the Gaofen series of Earth observation satellites has provided a wealth of high-quality data resources for agricultural remote sensing applications [12]. The GF-6 satellite, successfully launched in 2018, is China's first high-resolution satellite dedicated to precision agriculture observation [13,14]. It has a spatial resolution of 16 m and a revisit cycle of 4 days. Equipped with multispectral and hyperspectral cameras covering visible and near-infrared bands, it provides richer spectral and texture information for regional-scale agricultural remote sensing monitoring [12,15]. However, few researchers utilize GF-6 imagery for vineyard information extraction studies.

Currently, the remote sensing extraction of information related to tree fruit cultivation primarily relies on spectral features. For example, Zhu et al. [16] extracted the spatiotemporal changes in apple orchards from 2000 to 2017 based on the NDVI (Normalized Difference Vegetation Index) and phenological information, combining Sentinel-2, Landsat, and MODIS remote sensing data, and achieved an identification accuracy ( $R^2$ ) of 0.747. Similarly, the extraction of vineyard planting information, vegetation health status, and growth conditions is also achieved by analyzing spectral features [9,17]. Arab et al. [18] obtained distribution maps of grape growth stages and yield predictions based on Landsat 8 imagery, utilizing the NDVI, the LAI (Leaf Area Index), and the NDWI (Normalized Difference Water Index), and employed moving average and exponential smoothing methods. The results indicated that among all vegetation indices, the accuracy of NDVI in 2017 and 2019 was the highest ( $R^2 = 0.79$ ). In the study by Ferro et al. [19], different computer vision methods for canopy detection in vineyards using UAV multispectral images were compared. The results indicated that the coefficient of determination for Total Leaf Area (TLA) and NDVI data significantly improved for Mask R-CNN and U-Net. The NDVI data from the GMM (Gaussian Mixture Model) and SVM (Support Vector Machine) algorithms also showed a positive correlation. Regarding the correlation between leaf chlorophyll (Chl) and NDVI, both Mask R-CNN and U-Net methods demonstrated better performance.

As the research deepens, texture features, as derivative data from remote sensing imagery, can reveal the spatial variation patterns and spatial correlations of image grayscale. Scholars are gradually combining texture features with optical features for application in orchard extraction studies [20,21]. Song et al. [22] combined wavelet texture with spectral features to construct classification features based on QuickBird imagery. They

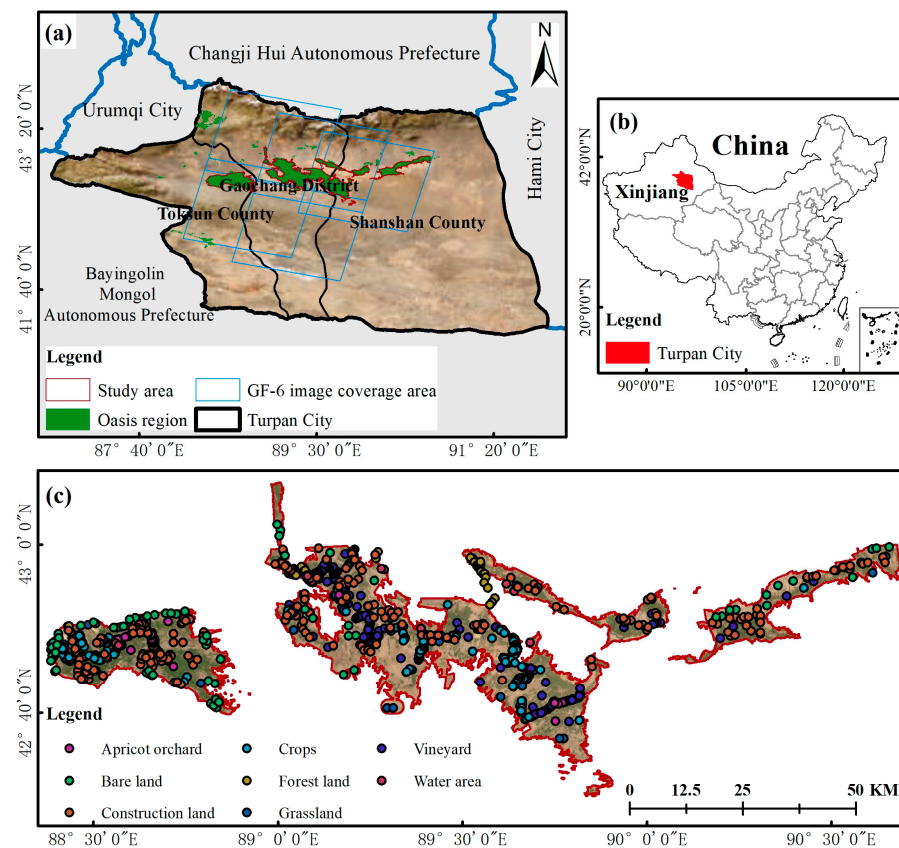
utilized the Random Forest classification algorithm to achieve land-use classification and extract the spatial distribution of kiwi orchards. The results indicated that the classification performance that integrated wavelet texture was the best, achieving an accuracy of 95.30%, which was significantly better than the results obtained using spectral features alone. Pu et al. [23] and Dian et al. [24] classified tree species and began to incorporate texture features to improve the accuracy of tree species classification. Yao et al. [25] used two scenes of high-resolution GF-2 remote sensing imagery from winter and summer as data sources. They combined NDVI and NDWI with texture features to construct a decision tree model based on spectral indices and texture features, successfully extracting the spatial distribution information of fruit trees in the study area for the year 2017. The overall classification accuracy was 89.57%, which represented improvements of 10.65% and 12.04% compared to the single spectral and texture models, respectively. The introduction of texture features can effectively capture the arrangement and density of leaves, thereby better distinguishing fruit-bearing plants from surrounding vegetation [24]. In complex forest and orchard environments, the overlap of vegetation and shadows often leads to confusion in spectral signals. However, texture features, due to their robustness against variations in lighting conditions, can mitigate these effects to a certain extent and improve extraction accuracy [22,25]. Currently, the main challenges in remote sensing identification of vineyards include the dense canopy structure and vertical growth, which complicate the acquisition and interpretation of remote sensing signals; additionally, overlapping and sprawling leaves exacerbate spectral signal confusion, and variations in lighting conditions lead to shadow interference [19,26]. These factors can result in individual pixels containing information from multiple ground objects, thereby affecting classification accuracy [27]. Therefore, incorporating texture features into the characteristics of vineyard remote sensing extraction is both necessary and worthy of further exploration.

Therefore, this study focuses on the main oasis area of Turpan City, utilizing GF-6 imagery to obtain the spectral and texture features of vineyards. First, the Boruta algorithm is employed to select the spectral and texture features that are sensitive, for vineyard information extraction. Next, machine learning algorithms, including Naive Bayes (NB), Support Vector Machine (SVM), and Random Forest (RF), are used to construct vineyard information extraction models that integrate both spectral and texture features. At the same time, the impact of different machine learning algorithms and remote sensing features on the accuracy of vineyard information extraction is compared. Ultimately, the aim is to provide technical references for remote sensing recognition and information extraction of vineyards and to offer data support for the development of the grape industry and the optimization of planting structures.

## 2. Materials and Methods

### 2.1. Study Area

The study area is located in Turpan City of Xinjiang Uyghur Autonomous Region, China ( $42^{\circ}57' N$ ,  $89^{\circ}11' E$ ), as shown in Figure 1. This region lies in an extremely arid desert zone, with desert areas accounting for 70% of the total area. The climate is extremely dry, with an average annual rainfall of only 33.8 mm. The soil is predominantly sandy and loamy, with low organic matter content and poor natural fertility due to the arid conditions. Therefore, oases have become the main areas for crop cultivation in the region [28,29]. Based on the distribution of oases in Turpan City [30] and considering the imaging quality of remote sensing data, the study area was selected to cover the main oasis regions of Turpan City. The primary fruit crop in the study area is grapes, followed by apricots. Other land cover types include farmland, grassland, and small areas of woodland.



**Figure 1.** Geographical Location of the Study Area and Distribution Map of Typical Ground Sample Points. (a) Geographical Location of the Study Area; (b) Location of Turpan City; (c) Distribution of Typical Ground Sample Points.

Grapes, as a perennial vine, bud in April and mature from late July to late September. In this region, grapevines are guided by trellises, with an average height of 3 to 4 m, and they are planted in rows, typically spaced 3.5 to 4 m apart. There is no natural vegetation or crop cover in the inter-row area. To maintain a proper distribution of the vines within the rows, regular pruning is required, resulting in a clearer and more orderly row distribution with tighter internal texture. In contrast, apricot trees, common perennial woody fruit trees in the region, bud in March and mature between late June and early August. Although they are also planted in rows, the spacing between rows is 2.5 to 3 m. The inter-row area does have natural vegetation or crop cover. Mature apricot trees have an average row height of 5 to 8 m, but since they rely on a woody trunk and branches to form a fixed tree shape, they are usually not pruned. This leads to a more diffuse row distribution and a relatively sparse internal structure.

## 2.2. Data Acquisition and Preprocessing

### 2.2.1. GF-6 Satellite Data

Based on the characteristics of vegetation phenology in the study area and the coverage of the imagery, this study selected GF-6 imagery from 12 to 24 October 2023 as the data source. At this time, the grapevines were in the EL (Eichhorn-Lorenz) 35–41 stage [31], while the grasslands had begun to wither, and most farmland was in a fallow state. This provided favorable conditions for the extraction of vineyards. To ensure the quality of the imagery, considerations such as the overpass time, weather conditions, and imaging effects were taken into account, resulting in the selection of five optimal images, with specific imaging times listed in Table 1.

**Table 1.** The specific imaging dates and quantities of the selected GF-6 imagery for the research area.

Imaging Time	Number
12 October 2023	2 scenes
16 October 2023	2 scenes
24 October 2023	1 scene

In the GF-6 imagery, the spatial resolution of the panchromatic imagery (PAN) is 2 m, while the spatial resolution of the multispectral imagery (PMS) is 8 m. The multispectral data consist of four bands: red, green, blue, and near infrared. The downloaded data were Level 1A data, which required preliminary processing for the multispectral data involving radiometric calibration, atmospheric correction, and orthorectification. Panchromatic images have higher spatial resolution, and by fusing them with multispectral images, higher resolution multispectral images can be generated, allowing for more precise identification and classification of land cover. The nearest neighbor interpolation algorithm is used to fuse panchromatic and multispectral images, resulting in a fused image with a spatial resolution of 2 m. All processing steps were completed in ENVI 5.6 (<https://portal.nv5geospatialsoftware.com>, accessed on 28 October 2024).

### 2.2.2. Ground Survey Data

The field sample point data were collected during an on-site survey in June–July 2023. To ensure the quality of the sample points despite the different dates of the ground survey and satellite data collection, we visually inspected all ground samples using high-resolution imagery from Google Earth. We excluded sample points where land cover types had changed due to the difference in dates between the ground survey and satellite data collection, as well as obviously incorrect samples (such as natural vegetation mistakenly labeled as crops) and samples located on roads or field boundaries. In total, there are 1068 valid sample points (Figure 1c), with the specific number of samples for each class shown in Table 2, with 70% of the sample points being used for constructing the vineyard extraction model and 30% being used for accuracy validation of the model. Based on GF-6 imagery, the optical characteristics, texture structures, and tonal variations in various land types in the study area were visually interpreted, creating a set of interpretation symbols specific to the land types in the study area (Table 2). This laid the foundation for the subsequent model construction [25].

**Table 2.** Information on different sample points and image features within the study area.



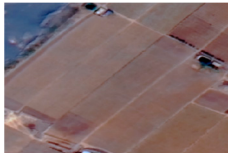

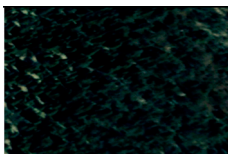

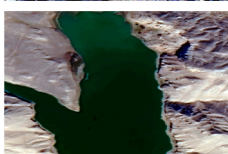

Land Type Names	Number of Sample Points/Points	Image Features and Interpretation Symbols	Example Images Under GF-6 Imagery
Vineyard	205	Strap-like distribution with relatively clear texture structure; most areas appear bright green, while a small portion is brown	
Apricot orchard	107	The texture structure is clear, with a strong grainy feel, exhibiting a regular plate-like distribution and appearing dark green	

Table 2. Cont.

Land Type Names	Number of Sample Points/Points	Image Features and Interpretation Symbols	Example Images Under GF-6 Imagery
Crops	216	The texture structure is clear and appears brown	
Grassland	79	Widely distributed and appears yellow	
Forest land	61	Irregular shape, densely distributed, and appears dark green	
Construction land	234	Distinct geometric shapes, distributed in patches, and appearing blue-white	
Water area	64	Sparse distribution with clear boundaries	
Bare land	102	Widely distributed and appears gray-brown	

### 2.3. Research Methodology

#### 2.3.1. Remote Sensing Feature Extraction Method

##### 1. Spectral Feature Extraction

Based on the latitude and longitude information of the sample plot centers, the sample points are mapped onto the remote sensing images, allowing for the extraction of the corresponding pixel remote sensing features. The NDVI is a commonly used important spectral feature in vineyard remote sensing. By reflecting the photosynthetic capacity and health status of vegetation, it provides an effective means for monitoring grape growth. NDVI effectively identifies and quantifies the vitality of the plant canopy by comparing the reflectance of red and near-infrared light. For grapes, high NDVI values are usually associated with favorable growing conditions and high photosynthetic efficiency, indicating healthy plants that help promote grape maturation and enhance yield [32–35]. The EVI is also an important spectral indicator used in vineyard remote sensing, aimed at improving the accuracy of monitoring vegetation cover and growth status. EVI effectively corrects for soil background and aerosol scattering effects by utilizing a combination of red, near-infrared, and blue wavelengths, thereby providing more accurate vegetation information. Due to the wide planting rows of grapes, EVI is particularly suitable for vineyards, which have complex canopy structures. The NDWI is an important spectral indicator for assessing water status in vineyards. It provides key information about the grape growth environment by analyzing the distribution of liquid water molecules within the plant canopy. High

NDWI values typically indicate sufficient water availability, reflecting healthy grape plants and favorable growing conditions [36,37]. In addition to the aforementioned spectral indices, the selected spectral features also included the red, green, blue, and near-infrared bands from the GF-6 imagery. Detailed information about the spectral features is provided in Table 3.

**Table 3.** Summary of selected optical feature information.

Type	Classification Features	Bands/Formula	Spectral Range
Spectral Bands	B1	Blue	0.45~0.52 $\mu\text{m}$
	B2	Green	0.52~0.60 $\mu\text{m}$
	B3	Red	0.63~0.69 $\mu\text{m}$
	B4	NIR	0.76~0.90 $\mu\text{m}$
Spectral Index	NDVI	$\frac{\text{NIR}-\text{Red}}{\text{NIR}+\text{Red}}$	
	EVI	$\frac{2.5 \times (\text{NIR}-\text{Red})}{\text{NIR}+6 \times \text{Red}-7.5 \times \text{Blue}+1}$	
	NDWI	$\frac{\text{Green}-\text{NIR}}{\text{Green}+\text{NIR}}$	

## 2. Texture Feature Extraction

Texture features consist of texture statistics and window size. Texture statistics reflect the spatial differences of objects and quantify the local texture structure of the image from different perspectives. The window size affects the completeness of the texture feature information and the performance of the gray-level co-occurrence matrix (GLCM) [38,39]. GLCM is a method for extracting texture features and is currently recognized as the most widely used texture statistical analysis method and texture measurement technique [40,41]. However, due to the large computational load of the gray-level co-occurrence matrix, this study only selected the eight texture statistical measures that performed best for remote sensing image classification for analysis [38–40] (Table 4).

**Table 4.** Texture features selected in the study.

Texture Statistics	Constructed Texture Features	
Mean (ME)	B1_ME *, B2_ME, B3_ME, B4_ME, NDVI_ME, EVI_ME, NDWI_ME	
Variance (VA)	B1_VA, B2_VA, B3_VA, B4_VA, NDVI_VA, EVI_VA, NDWI_VA	
Homogeneity (HO)	B1_HO, B2_HO, B3_HO, B4_HO, NDVI_HO, EVI_HO, NDWI_HO	The window sizes are set to 3 $\times$ 3, 5 $\times$ 5, 7 $\times$ 7, 9 $\times$ 9, 11 $\times$ 11, 13 $\times$ 13, and 15 $\times$ 15.
Contrast (CO)	B1_CO, B2_CO, B3_CO, B4_CO, NDVI_CO, EVI_CO, NDWI_CO	
Dissimilarity (DI)	B1_DI, B2_DI, B3_DI, B4_DI, NDVI_DI, EVI_DI, NDWI_DI	
Entropy (EN)	B1_EN, B2_EN, B3_EN, B4_EN, NDVI_EN, EVI_EN, NDWI_EN	
Angular Second Moment (ASM)	B1_ASM, B2_ASM, B3_ASM, B4_ASM, NDVI_ASM, EVI_ASM, NDWI_ASM	
Correlation (COR)	B1_COR, B2_COR, B3_COR, B4_COR, NDVI_COR, EVI_COR, NDWI_COR	

\* Examples of abbreviation meanings: B1\_ME represents the mean statistic of the B1 band.

The window size directly affects the integrity of texture feature information and the performance of the GLCM. A window that is too small fails to adequately represent the features of the object, while a window that is too large may incorporate texture features from other objects. Therefore, selecting an appropriate window size is also crucial [42,43]. This study set the moving window sizes to commonly used dimensions of 3  $\times$  3, 5  $\times$  5,

$7 \times 7$ ,  $9 \times 9$ ,  $11 \times 11$ ,  $13 \times 13$ , and  $15 \times 15$  (Table 4). At the same time, the default angle of 0 degrees and a pixel interval of 1 were used for texture calculations.

### 2.3.2. Remote Sensing Feature Importance Evaluation Method

This study used the Boruta algorithm to analyze the importance of remote sensing features. Boruta is an effective method specifically designed for selecting key features from high-dimensional data. It is suitable for handling large datasets and complex features, significantly improving model performance [44,45]. The working principle of the Boruta algorithm includes the following steps: First, it copies each real feature and randomly shuffles it to generate a set of “shadow” features. Then, a model is trained to evaluate the importance of both the original features and the shadow features. Finally, the score of each real feature is compared with the highest score among the shadow features to determine its contribution. If the importance of a real feature is significantly higher than that of the shadow features, it is considered an effective feature; otherwise, it is deemed irrelevant [46,47]. By analyzing the importance of remote sensing features, sensitive remote sensing features for vineyard identification are selected, and the sensitivity of various texture statistics to vineyard recognition is examined under different window sizes. This plays a crucial role in constructing the vineyard identification model.

### 2.3.3. Vineyard Information Extraction Model Construction Approach

Based on the important remote sensing features identified for vineyard recognition, we constructed three vineyard information extraction models that integrate both spectral and texture features using Naive Bayes (NB), Support Vector Machine (SVM), and Random Forest (RF) algorithms. These models are the NB model based on spectral and texture features (M1), the SVM model based on spectral and texture features (M2), and the RF model based on spectral and texture features (M3). By evaluating the performance of these three models, the best algorithm was determined. Subsequently, the impact of different combinations of remote sensing features on the accuracy of vineyard information extraction was compared using the selected optimal algorithm.

The classification principle of NB is based on the prior probabilities of an object. It uses Bayes’ theorem to calculate the posterior probabilities and selects the class with the highest posterior probability as the class to which the object belongs [48]. The NB classification not only allows all attributes of the test samples to participate in the classification but also has a wide applicability for the distribution of sample attributes [49]. SVM is a machine learning method based on statistical learning theory [50]. It automatically identifies support vectors that have a significant distinction for classification, thereby constructing a classifier that maximizes the margin between classes, resulting in good generalization and high classification accuracy [51]. RF is an ensemble learning method that performs classification and regression tasks by constructing multiple decision trees [52]. It determines the final prediction result through voting or averaging the outcomes. RF can handle complex remote sensing image classification and is suitable for multiple classes and features [53].

### 2.3.4. Accuracy Verification Method

This study employed a confusion matrix to evaluate the accuracy of the model’s extraction results. The confusion matrix, also known as the error matrix, is a standard format for representing accuracy evaluation [54]. This study selected five validation metrics—Kappa coefficient, classification accuracy (CA), classification Error (CE), and omission error (OE)—to reflect the accuracy of vineyard classification [54,55].

$$CA = 1/2 \left( \frac{n_{ii}}{n_i} + \frac{n_{ii}}{n_i} \right) \times 100\%, \quad (1)$$

$$Kappa = \frac{\left[ n \cdot \sum_{i=1}^q n_{ii} - \sum_{i=1}^q (n_i \times n_i) \right]}{\left[ n^2 - \sum_{i=1}^q (n_i \times n_i) \right]}, \quad (2)$$



$$CE = \frac{n_{i.} - n_{ii}}{n_{i.}} \times 100\%, \tag{3}$$

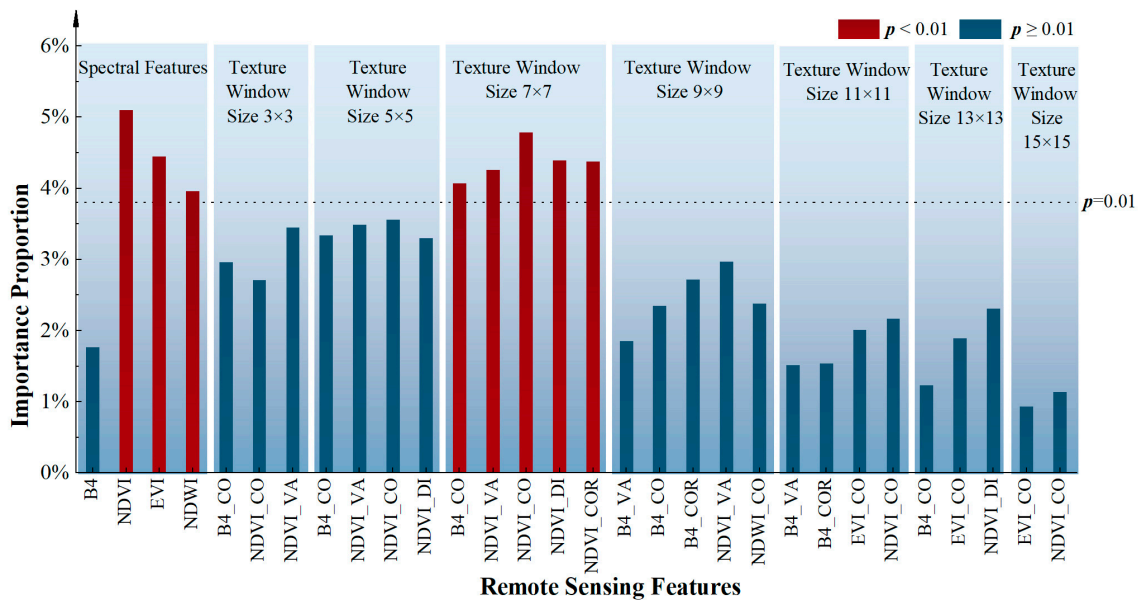
$$OE = \frac{n_{.i} - n_{ii}}{n_{.i}} \times 100\%, \tag{4}$$

Here,  $n_{ii}$  represents the value in the  $i$ -th row and  $i$ -th column of the confusion matrix,  $n_{i.}$  is the sum of the  $i$ -th row of the confusion matrix,  $n_{.i}$  is the sum of the  $i$ -th column of the confusion matrix,  $n$  is the total number of validation samples, and  $q$  is the number of rows and columns in the confusion matrix.

### 3. Results

#### 3.1. Importance Analysis of Remote Sensing Features for Vineyard Extraction

Based on ground survey sample points, optical and texture features were extracted from the GF-6 data. The Boruta algorithm was then applied to obtain the importance scores of the features, which were subsequently normalized. The results are illustrated in Figure 2. The figure only displays the remote sensing features that have  $p \leq 0.05$  and are greater than the shadow variable. Among the spectral information, the importance proportion of the NDVI index is 5.10%, followed by the EVI index at 4.45%, and then the NDWI at 3.96%. Furthermore, all of them passed the 0.01 significance check.



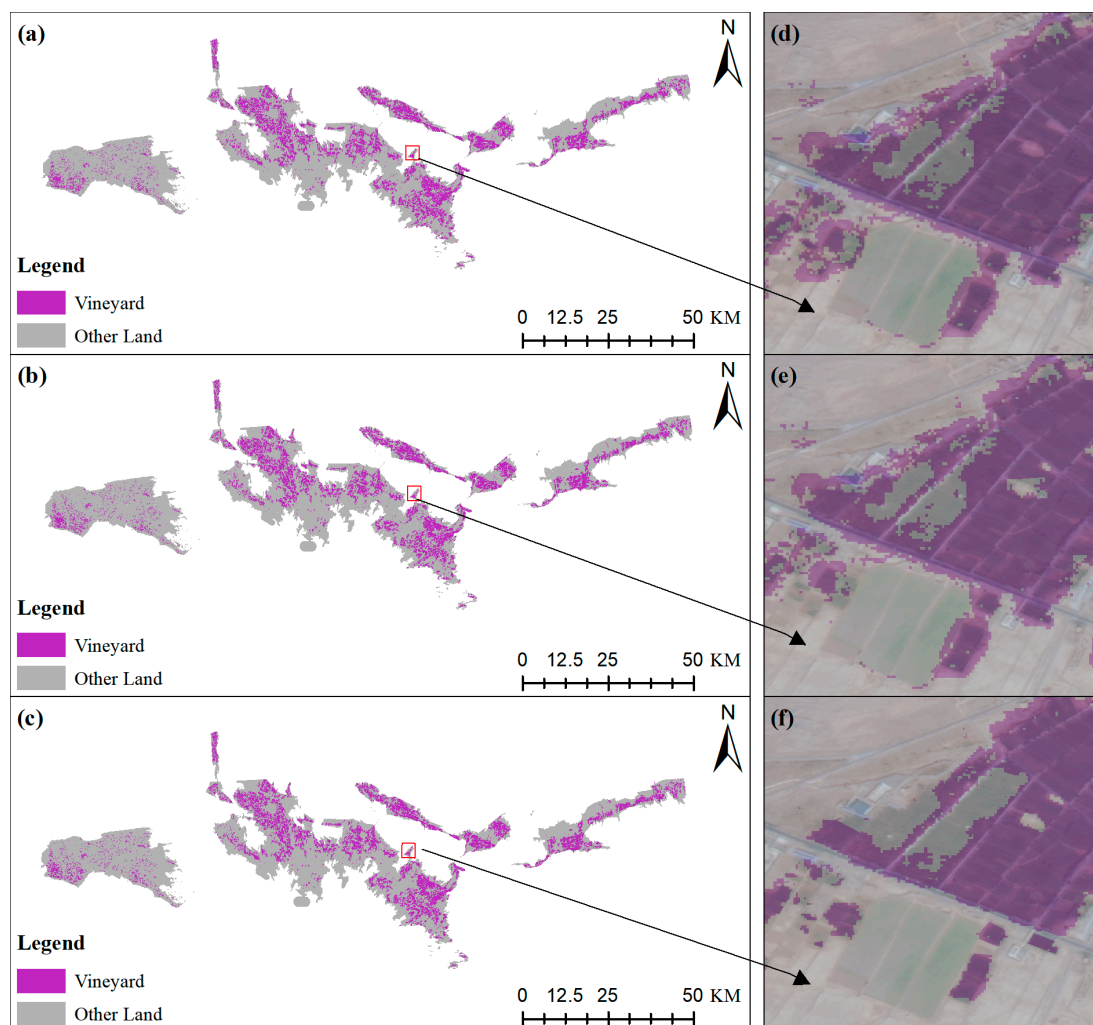
**Figure 2.** Importance of Various Remote Sensing Features (the figure only displays remote sensing features that have  $p \leq 0.05$  and are greater than the shadow variable).

In the texture feature statistics, contrast (CO), variance (VA), correlation (COR), and dissimilarity (DI) have greater importance for vineyard extraction. Particularly, when the window size is  $7 \times 7$ , the statistical measures NDVI\_CO and NDVI\_VA reflect the highest importance for crop extraction, with NDVI\_CO showing more stability across different window sizes. Additionally, the size of the texture window has a significant impact on importance. As the window size increases, the importance first rises and then declines. When the window size is  $7 \times 7$ , the importance reaches its maximum and passes the 0.01 significance check. The best-performing features at this size include B4\_CO, NDVI\_VA, NDVI\_CO, NDVI\_DI, and NDVI\_COR.

Based on this, a total of eight sensitive features were selected: three spectral features, including NDVI, EVI, and NDWI; and five texture features, all derived from a  $7 \times 7$  window, including B4\_CO, NDVI\_VA, NDVI\_CO, NDVI\_DI, and NDVI\_COR.

### 3.2. Vineyard Extraction Model Performance Evaluation

The vineyard classification results of the three models (M1, M2, M3) for vineyard information extraction that integrate both spectral and texture features are shown in Figure 3. Figure 3a–c shows the overall distribution of vineyards under the three models, all indicating that the central oasis area of the study region has a higher coverage of vineyards, while the western and eastern areas have less coverage. However, in the enlarged local images (Figure 3d–f), it can be observed that there are still differences in the classification results of each model. The M1 model performs relatively poorly in identifying vineyards, with a scattered distribution of patches, a high number of misclassifications, and a significant presence of omissions within the vineyard areas, leading to unsatisfactory classification results. The M2 model improves the recognition effect compared with the M1 model, the wrong score is obviously reduced, but the omission is still more obvious, and the classification boundary is slightly fuzzy. The M3 model has the best extraction effect, the classification results are more continuous and concentrated, the wrong score and omission are minimized, and the boundary of the vineyard is clear. This is because, compared with other algorithms, RF performs well in the complex remote sensing image classification task, especially suitable for multi-category and multi-feature classification situations [52,53].



**Figure 3.** Extraction Results of Vineyards from Different Models. (a) M1 Model Extraction Results; (b) M2 Model Extraction Results; (c) M3 Model Extraction Results; (d) Local Image of M1 Model Extraction Results; (e) Local Image of M2 Model Extraction Results; (f) Local Image of M3 Model Extraction Results.

The accuracy of the three models was also calculated using the confusion matrix, as shown in Table 5. The results show that the M3 model outperformed the M2 and M1 models, achieving an accuracy of 93.89% for vineyard identification, with a Kappa coefficient of 0.89, a misclassification error of 8.11%, and an omission error of 4.11%. Compared to the M1 model, the M3 model improved vineyard identification accuracy by 12.25%, raised the Kappa coefficient by 0.11, reduced the misclassification error by 6.93%, and decreased the omission error by 17.57%. In comparison with the M2 model, the M3 model increased vineyard identification accuracy by 8.02%, enhanced the Kappa coefficient by 0.06, lowered the misclassification error by 2.46%, and reduced the omission error by 13.58%. Overall, the RF algorithm (M3) demonstrated stronger adaptability in the complex environment of the study area, with significantly higher classification accuracy than the other two models.

**Table 5.** The extraction accuracy results of vineyards using three different algorithm models constructed based on spectral and texture features.

Model	Name	Algorithm	Feature	Kappa Coefficient	Vineyard Classification Accuracy (%)	Vineyard Classification Error (%)	Vineyard Omission Error (%)
M1	The NB Model Integrating Spectral and Texture Features	Naive Bayes	Spectral Features: NDVI, EVI, and NDWI.	0.78	81.64	15.04	21.68
M2	The SVM Model Integrating Spectral and Texture Features	Support Vector Machine	Texture Features: B4_CO, NDVI_VA, NDVI_CO, NDVI_DI, and NDVI_COR under a 7 × 7 window	0.83	85.87	10.57	17.69
M3	The RF Model Integrating Spectral and Texture Features	Random Forest		0.89	93.89	8.11	4.11

### 3.3. The Influence of Spectral and Texture Features on Vineyard Extraction Accuracy

From Table 5, it can be seen that the RF model (M3) that integrates spectral and texture features is optimal for vineyard information extraction. To compare the impact of single spectral features, single texture features, and the combined spectral and texture features on vineyard extraction accuracy, an RF model based on single spectral features (M4) and an RF model based on single texture features (M5) were further constructed based on the optimal RF algorithm. The accuracy of vineyard information extraction for M3, M4, and M5 was then compared, and the results are shown in Table 6. It is clear that the M3 model, which combines spectral and texture features, significantly outperforms the M4 model based on single spectral features and the M5 model based on single texture features in vineyard identification. The M3 model shows a 13.59% increase in accuracy compared to the M4 model, with a Kappa coefficient increase of 0.12, a reduction in misclassification error of 6.86%, and a decrease in omission error of 20.2%. When compared to the M5 model, the M3 model demonstrates a 14.92% improvement in classification accuracy, a Kappa coefficient increase of 0.21, a 17.00% reduction in misclassification error, and a 17.24% decrease in omission error. In summary, the integration of both spectral and texture features enables a more comprehensive capture of vineyard characteristics, thereby enhancing overall classification accuracy and reducing both misclassification and omission errors.

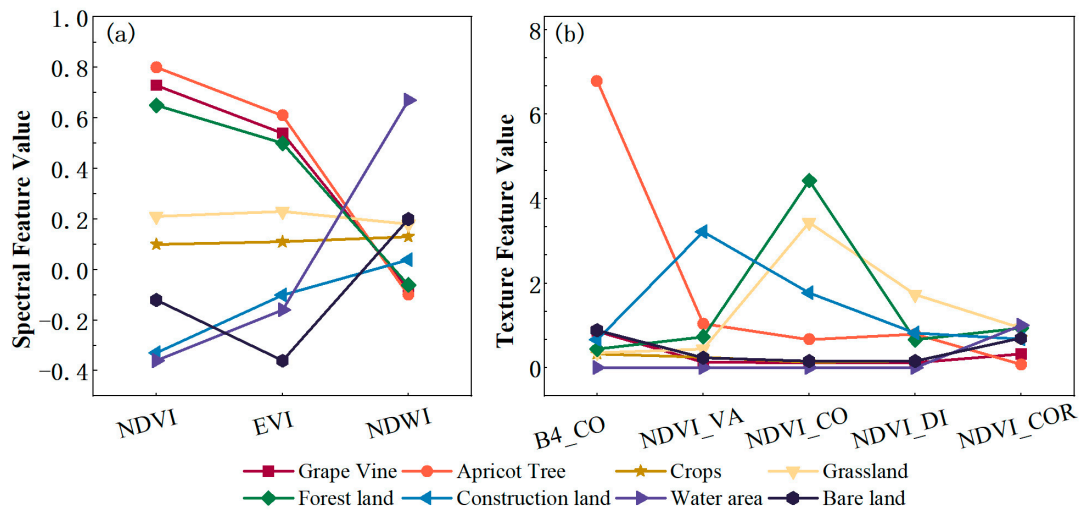
**Table 6.** The extraction accuracy results of vineyards using three Random Forest models constructed based on different remote sensing features.

Model	Name	Feature	Kappa Coefficient	Vineyard Classification Accuracy (%)	Vineyard Classification Error (%)	Vineyard Omission Error (%)
M3	The RF Model Integrating Spectral and Texture Features	Spectral Features: NDVI, EVI, and NDWI. Texture Features: B4_CO, NDVI_VA, NDVI_CO, NDVI_DI, and NDVI_COR under a $7 \times 7$ window.	0.89	93.89	8.11	4.11
M4	The RF Model with Single Spectral Feature	Spectral Features: NDVI, EVI, and NDWI.	0.77	80.36	14.97	24.31
M5	The RF Model with Single Texture Feature	Texture Features: B4_CO, NDVI_VA, NDVI_CO, NDVI_DI, and NDVI_COR under a $7 \times 7$ window.	0.68	76.77	25.11	21.35

#### 4. Discussion

This study employed three algorithms for grape extraction, revealing significant differences among them. The NB algorithm struggles to adequately capture the correlations between spectral and texture features due to its assumption of independence among features [56]. This assumption may adversely affect classification performance in vineyard extraction, leading to decreased accuracy. While the SVM algorithm excels in processing high-dimensional data, its training complexity is relatively high, particularly when dealing with large data dimensions or sample sizes [57]. For the complex task of vineyard extraction, feature selection and parameter optimization (such as kernel function selection) are crucial. If parameters are improperly selected, SVM may fail to effectively distinguish vineyards from other vegetation types. Additionally, SVM is sensitive to noise, which can also impact classification accuracy [58]. The RF algorithm demonstrates outstanding performance in integrating spectral and texture features, effectively leveraging various remote sensing characteristics to enhance classification accuracy [59,60]. However, RF may face the risk of overfitting when applied to high-dimensional datasets. Furthermore, existing studies have indicated that RF's classification accuracy may decrease when processing sub-meter resolution imagery [61]. In contrast, RF has shown greater stability in the 2 m or higher resolution imagery used in this study. Therefore, future research should further explore the performance differences of RF across various image resolutions to optimize vineyard extraction outcomes.

From the analysis of different remote sensing features on vineyard extraction results, it is evident that models integrating both spectral and texture features significantly outperform those using only a single feature. As shown in Figure 4a, for vegetation similar to grapevines, apricot trees, and forests, similarities in physiological structure, leaf morphology, and canopy characteristics often lead to overlapping or closely resembling spectral reflectance features [62,63]. This indicates that a single spectral feature cannot comprehensively reflect the internal differences among these fruit-bearing objects, making precise classification challenging. The vineyard's regular row spacing, strip-like distribution, and the directional arrangement of plants create a distinct texture pattern, which provides a strong differentiation compared to other fruit trees or vegetation (Figure 4b). Although texture features have advantages in capturing the details of vineyards versus other fruit-bearing vegetation, using texture information alone is insufficient to accurately distinguish vineyards from other non-vegetated objects, such as bare soil. Therefore, combining spectral and texture features can compensate for each other's shortcomings and fully leverage the informational strengths of both dimensions. This conclusion aligns with findings from previous studies on fruit-bearing crops [23–25].



**Figure 4.** Main Remote Sensing Feature Values of the Study Area. (a) Main Spectral Feature Values of Land Cover; (b) Main Texture Feature Values of Land Cover.

Grapes, as perennial climbing plants, are cultivated using trellises, creating regular row spacing and strip-like distribution patterns. Low-resolution satellite imagery cannot clearly capture details such as row spacing and trellis structure in vineyards [64]. With the advancement of drone technology, sub-centimeter resolution imagery can now be obtained, allowing researchers to clearly capture these features. However, studies have shown that drone imagery for vineyard classification is still affected by the projection of canopy shadows and the background between rows of grapevines, while this impact is relatively minimal in low-resolution satellite imagery [19]. The 2 m resolution imagery from GF-6 used in this study can not only capture the fine structural features of vineyards clearly [12] but also effectively reduce classification errors caused by canopy shadows and background between rows. Additionally, this study found that incorporating texture features significantly improves the extraction accuracy of vineyards. Texture features exhibit strong robustness against variations in lighting, which can help eliminate spectral signal confusion caused by overlapping vegetation and shadows, thus enhancing extraction accuracy [22,25]. These findings provide new insights for further research.

The methods employed in this study also have certain limitations. First, in feature selection, only the Boruta algorithm was used, which is relatively singular. Second, we generated a 2 m high-resolution multispectral image from fused images. Although this improved the precision of land feature identification and classification, some potential issues remain. Despite the ability of the fused multispectral image to capture more details, noise and interference in complex vegetation-covered areas may affect classification accuracy, and artifacts may be introduced during the fusion process, leading to feature confusion. Finally, the inconsistency between the satellite data collection date and the ground sampling time is also an issue. Although Google imagery was used to analyze point changes over time and delete the changed points, from the perspective of experimental rigor, the satellite data collection date should align with the ground sampling time. Therefore, in future research, we will consider using GF-2 satellite imagery, employing more diverse feature selection methods, and ensuring that the satellite data collection date is as close as possible to the ground sampling time.

## 5. Conclusions

This study focused on the main oasis area of Turpan City in Xinjiang, China. Using high-resolution GF-6 imagery, the research employed machine learning algorithms such as Naive Bayes (NB), Support Vector Machine (SVM), and Random Forest (RF) to develop models for the extraction of vineyard information by integrating spectral and texture features. The results indicate that three spectral features and five texture features under

a  $7 \times 7$  window exhibit significant sensitivity to vineyard recognition following feature selection via the Boruta algorithm. These spectral features include Normalized Difference Vegetation Index (NDVI), Enhanced Vegetation Index (EVI), and Normalized Difference Water Index (NDWI), while texture features include contrast statistics in the near-infrared band (B4\_CO) and the variance statistic, contrast statistic, heterogeneity statistic, and correlation statistic derived from NDVI images (NDVI\_VA, NDVI\_CO, NDVI\_DI, and NDVI\_COR). The RF algorithm significantly outperforms both the NB and SVM models in extracting vineyard information, achieving an accuracy of 93.89% and a Kappa coefficient of 0.89. This represents a notable improvement of 12.25% in accuracy and 0.11 in the Kappa coefficient over the NB model, and an improvement of 8.02% in accuracy and 0.06 in the Kappa coefficient compared to the SVM model. Models that incorporate both spectral and texture features significantly outperform their single-feature counterparts, suggesting that the fusion of these characteristics more effectively captures the spatial distribution characteristics of vineyards. This finding would provide an important theoretical basis and methodological reference for the application of remote sensing technology in the agricultural field.

**Author Contributions:** Conceptualization, X.H. and H.Y.; methodology, X.H. and H.Y.; software, X.H. and C.N.; validation, X.H., C.N. and Y.Z.; formal analysis, X.H. and H.Y.; investigation, X.H., C.N. and Y.Z.; resources, C.N.; data curation, X.H. and C.N.; writing—original draft preparation, X.H.; writing—review and editing, X.H. and H.Y.; visualization, X.H.; supervision, Y.Z. and F.W.; project administration, X.H. and F.W.; funding acquisition, H.Y. All authors have read and agreed to the published version of the manuscript.

**Funding:** This research was funded by the Third Xinjiang Scientific Expedition Program of China (Grant No. 2022xjkk1100), the Natural Science Foundation of Xinjiang Uygur Autonomous Region, China (2024D01A21); the Youth Innovation Promotion Association CAS (No. 2021119); and the Future Star Talent Program of Aerospace Information Research Institute, Chinese Academy of Sciences (No. 2020 KTYWLZX08).

**Data Availability Statement:** The raw data supporting the conclusions of this article will be made available by the authors on request.

**Acknowledgments:** The authors sincerely thank the editor and anonymous reviewers for their valuable comments and suggestions to improve the quality of this paper.

**Conflicts of Interest:** The authors declare no conflicts of interest.

## References

1. Canton, H. Food and agriculture organization of the United Nations—FAO. In *The Europa Directory of International Organizations 2021*; Routledge: London, UK, 2021; pp. 297–305.
2. Gao, W.; Qiu, Q.; Yuan, C.; Shen, X.; Cao, F.; Wang, G.; Wang, G. Forestry big data: A review and bibliometric analysis. *Forests* **2022**, *13*, 1549. [[CrossRef](#)]
3. López-Pérez, E.; Sanchis-Ibor, C.; Jiménez-Bello, M.Á.; Pulido-Velazquez, M. Mapping of irrigated vineyard areas through the use of machine learning techniques and remote sensing. *Agric. Water Manag.* **2024**, *302*, 108988. [[CrossRef](#)]
4. Meng, X.; Rao, Y.; Tao, T.; Dong, S.; Jia, A.L.; Ma, H. A review of plant breeders' rights application and granting for fruit trees in China from 2000 to 2019. *Sci. Hortic.* **2021**, *276*, 109749. [[CrossRef](#)]
5. Xia, C.; Liu, Z.; Suo, X.; Cao, S. Quantifying the net benefit of land use of fruit trees in China. *Land Use Policy* **2020**, *90*, 104276. [[CrossRef](#)]
6. Zhou, X.-X.; Li, Y.-Y.; Luo, Y.-K.; Sun, Y.-W.; Su, Y.-J.; Tan, C.-W.; Liu, Y.-J. Research on remote sensing classification of fruit trees based on Sentinel-2 multi-temporal imageries. *Sci. Rep.* **2022**, *12*, 11549. [[CrossRef](#)] [[PubMed](#)]
7. Tang, H.; Wu, W.; Yang, P.; Zhou, Q.; Chen, Z. Recent progresses in monitoring crop spatial patterns by using remote sensing technologies. *Sci. Agric. Sin.* **2010**, *43*, 2879–2888.
8. Chen, Z.; Ren, J.; Tang, H.; Shi, Y.; Liu, J. Progress and perspectives on agricultural remote sensing research and applications in China. *J. Remote Sens.* **2016**, *20*, 748–767.
9. Matese, A.; Di Gennaro, S.; Miranda, C.; Berton, A.; Santesteban, L. Evaluation of spectral-based and canopy-based vegetation indices from UAV and Sentinel 2 images to assess spatial variability and ground vine parameters. *Adv. Anim. Biosci.* **2017**, *8*, 817–822. [[CrossRef](#)]

10. Peña, J.M.; Gutiérrez, P.A.; Hervás-Martínez, C.; Six, J.; Plant, R.E.; López-Granados, F. Object-based image classification of summer crops with machine learning methods. *Remote Sens.* **2014**, *6*, 5019–5041. [[CrossRef](#)]
11. Foerster, S.; Kaden, K.; Foerster, M.; Itzerott, S. Crop type mapping using spectral–temporal profiles and phenological information. *Comput. Electron. Agric.* **2012**, *89*, 30–40. [[CrossRef](#)]
12. Xia, T.; He, Z.; Cai, Z.; Wang, C.; Wang, W.; Wang, J.; Hu, Q.; Song, Q. Exploring the potential of Chinese GF-6 images for crop mapping in regions with complex agricultural landscapes. *Int. J. Appl. Earth Obs. Geoinf.* **2022**, *107*, 102702. [[CrossRef](#)]
13. Deng, Z.; Lu, Z.; Wang, G.; Wang, D.; Ding, Z.; Zhao, H.; Xu, H.; Shi, Y.; Cheng, Z.; Zhao, X. Extraction of fractional vegetation cover in arid desert area based on Chinese GF-6 satellite. *Open Geosci.* **2021**, *13*, 416–430. [[CrossRef](#)]
14. Jiang, X.; Fang, S.; Huang, X.; Liu, Y.; Guo, L. Rice mapping and growth monitoring based on time series GF-6 images and red-edge bands. *Remote Sens.* **2021**, *13*, 579. [[CrossRef](#)]
15. Kang, Y.; Meng, Q.; Liu, M.; Zou, Y.; Wang, X. Crop classification based on red edge features analysis of GF-6 WFV data. *Sensors* **2021**, *21*, 4328. [[CrossRef](#)] [[PubMed](#)]
16. Zhu, Y.; Yang, G.; Yang, H.; Wu, J.; Lei, L.; Zhao, F.; Fan, L.; Zhao, C. Identification of apple orchard planting year based on spatiotemporally fused satellite images and clustering analysis of foliage phenophase. *Remote Sens.* **2020**, *12*, 1199. [[CrossRef](#)]
17. Zheng, Y.; Sarigul, E.; Panicker, G.; Stott, D. Vineyard LAI and canopy coverage estimation with convolutional neural network models and drone pictures. In Proceedings of the Sensing for Agriculture and Food Quality and Safety XIV, Orlando, FL, USA, 1 June 2022; pp. 29–38.
18. Arab, S.T.; Noguchi, R.; Matsushita, S.; Ahamed, T. Prediction of grape yields from time-series vegetation indices using satellite remote sensing and a machine-learning approach. *Remote Sens. Appl. Soc. Environ.* **2021**, *22*, 100485. [[CrossRef](#)]
19. Ferro, M.V.; Sørensen, C.G.; Catania, P. Comparison of different computer vision methods for vineyard canopy detection using UAV multispectral images. *Comput. Electron. Agric.* **2024**, *225*, 109277. [[CrossRef](#)]
20. Kulikova, M.S.; Mani, M.; Srivastava, A.; Descombes, X.; Zerubia, J. Tree species classification using radiometry, texture and shape based features. In Proceedings of the 2007 15th European Signal Processing Conference, Poznań, Poland, 3–7 September 2007; pp. 1595–1599.
21. Othmani, A.; Piboule, A.; Dalmau, O.; Lomenie, N.; Mokrani, S.; Voon, L.F.C.L.Y. Tree species classification based on 3D bark texture analysis. In *Proceedings of the Image and Video Technology: 6th Pacific-Rim Symposium, PSIVT 2013, Guanajuato, Mexico, 28 October–1 November 2013*; Proceedings 6; Springer: Berlin/Heidelberg, Germany, 2014; pp. 279–289.
22. Song, R.; Ning, J.; Chang, Q.; Ban, S.; Liu, X.; Zhang, H. Kiwifruit orchard mapping based on wavelet textures and random forest. *Trans. Chin. Soc. Agric. Mach.* **2018**, *49*, 222–231.
23. Pu, R.; Landry, S. A comparative analysis of high spatial resolution IKONOS and WorldView-2 imagery for mapping urban tree species. *Remote Sens. Environ.* **2012**, *124*, 516–533. [[CrossRef](#)]
24. Dian, Y.; Li, Z.; Pang, Y. Spectral and texture features combined for forest tree species classification with airborne hyperspectral imagery. *J. Indian Soc. Remote Sens.* **2015**, *43*, 101–107. [[CrossRef](#)]
25. Yao, X.; Jin, J.; Xu, F.; Feng, X.; Luo, M.; Bi, L.; Lu, Z. Research on spectral and texture feature selection for fruit tree extraction in the Taihu Lake Basin. *Chin. J. Eco-Agric.* **2019**, *27*, 1596–1606.
26. Garofalo, S.P.; Intrigliolo, D.S.; Camposeo, S.; Alhaji Ali, S.; Tedone, L.; Lopriore, G.; De Mastro, G.; Vivaldi, G.A. Agronomic responses of grapevines to an irrigation scheduling approach based on continuous monitoring of soil water content. *Agronomy* **2023**, *13*, 2821. [[CrossRef](#)]
27. Pérez, D.S.; Bromberg, F.; Diaz, C.A. Image classification for detection of winter grapevine buds in natural conditions using scale-invariant features transform, bag of features and support vector machines. *Comput. Electron. Agric.* **2017**, *135*, 81–95. [[CrossRef](#)]
28. Wang, Y. Oasis ecosystem and its environmental characteristics. *Arid Land Geogr.* **2000**, *23*, 7–12.
29. Wang, X.; Hu, W.; Chang, Y.; Gao, C. Dynamic monitoring of ecological environment of Ejina Banner Oasis using remote sensing technology (1986 to 2000). In Proceedings of the Ecosystems Dynamics, Ecosystem-Society Interactions, and Remote Sensing Applications for Semi-Arid and Arid Land, Hangzhou, China, 24–27 October 2002; pp. 599–603.
30. National Cryosphere Desert Data Center. Available online: <http://www.ncdc.ac.cn/portal/metadata/2ee6aa92-0747-4e00-abbe-c48c60f84737> (accessed on 25 October 2024).
31. Lorenz, D.; Eichhorn, K.; Bleiholder, H.; Klose, R.; Meier, U.; Weber, E. Growth Stages of the Grapevine: Phenological growth stages of the grapevine (*Vitis vinifera* L. ssp. *vinifera*)—Codes and descriptions according to the extended BBCH scale. *Aust. J. Grape Wine Res.* **1995**, *1*, 100–103. [[CrossRef](#)]
32. Sellers, P.J. Canopy reflectance, photosynthesis and transpiration. *Int. J. Remote Sens.* **1985**, *6*, 1335–1372. [[CrossRef](#)]
33. Lamb, D.W.; Weedon, M.; Bramley, R. Using remote sensing to predict grape phenolics and colour at harvest in a Cabernet Sauvignon vineyard: Timing observations against vine phenology and optimising image resolution. *Aust. J. Grape Wine Res.* **2004**, *10*, 46–54. [[CrossRef](#)]
34. Meggio, F.; Zarco-Tejada, P.J.; Núñez, L.C.; Sepulcre-Cantó, G.; González, M.; Martín, P. Grape quality assessment in vineyards affected by iron deficiency chlorosis using narrow-band physiological remote sensing indices. *Remote Sens. Environ.* **2010**, *114*, 1968–1986. [[CrossRef](#)]
35. Rouse, J.W.; Haas, R.H.; Schell, J.A.; Deering, D.W. *Monitoring Vegetation Systems in the Great Plains with ERTS*; NASA Special Publications: Washington, DC, USA, 1974; Volume 351, p. 309.

36. Sun, L.; Gao, F.; Anderson, M.C.; Kustas, W.P.; Alsina, M.M.; Sanchez, L.; Sams, B.; McKee, L.; Dulaney, W.; White, W.A. Daily mapping of 30 m LAI and NDVI for grape yield prediction in California vineyards. *Remote Sens.* **2017**, *9*, 317. [[CrossRef](#)]
37. Zhao, X.; Jing, X.; Wang, L.; Liu, Y.; Xu, X. Grape remote sensing recognition based on GF-1/WFV time series. *J. Henan Agric. Sci.* **2019**, *48*, 153–160.
38. Feng, J.; Yang, Y.J. Study of texture images extraction based on gray level cooccurrence matrix. *Beijing Surv. Mapp.* **2007**, *3*, 19–22.
39. Li, L.H.; Jia, X.M.; Zhang, J.T. Research on extraction and assistant classification of remote sensing for texture feature. *Adv. Mater. Res.* **2015**, *1073*, 1881–1885. [[CrossRef](#)]
40. Bradley, A.; Jackway, P.; Lovell, B. Classification in scale-space: Applications to texture analysis. In Proceedings of the International Conference on Information Processing in Medical Imaging, Ile de Berder, France, 26–30 June 1995; pp. 375–376.
41. Walker, R.; Jackway, P.; Longstaff, I. Recent developments in the use of the co-occurrence matrix for texture recognition. In Proceedings of the 13th International Conference on Digital Signal Processing, Santorini, Greece, 2–4 July 1997; pp. 63–65.
42. Guo, D.; Song, Z. A study on texture image classifying based on gray-level co-occurrence matrix. *For. Mach. Woodwork. Equip.* **2005**, *33*, 21–23.
43. Ren, G.; Jiang, T. Study on GLCM-based texture extraction methods. *Comput. Appl. Softw.* **2014**, *31*, 190–325.
44. Kursu, M.B.; Jankowski, A.; Rudnicki, W.R. Boruta—a system for feature selection. *Fundam. Inform.* **2010**, *101*, 271–285. [[CrossRef](#)]
45. Kursu, M.B.; Rudnicki, W.R. Feature selection with the Boruta package. *J. Stat. Softw.* **2010**, *36*, 1–13. [[CrossRef](#)]
46. Anand, N.; Sehgal, R.; Anand, S.; Kaushik, A. Feature selection on educational data using Boruta algorithm. *Int. J. Comput. Intell. Stud.* **2021**, *10*, 27–35. [[CrossRef](#)]
47. Maurya, N.S.; Kushwah, S.; Kushwaha, S.; Chawade, A.; Mani, A. Prognostic model development for classification of colorectal adenocarcinoma by using machine learning model based on feature selection technique boruta. *Sci. Rep.* **2023**, *13*, 6413.
48. Chen, S.; Webb, G.I.; Liu, L.; Ma, X. A novel selective naïve Bayes algorithm. *Knowl.-Based Syst.* **2020**, *192*, 105361. [[CrossRef](#)]
49. Hall, M. A decision tree-based attribute weighting filter for naïve Bayes. In Proceedings of the International Conference on Innovative Techniques and Applications of Artificial Intelligence, Cambridge, UK, 18 December 2006; pp. 59–70.
50. Pisner, D.A.; Schnyer, D.M. Support vector machine. In *Machine Learning*; Elsevier: Amsterdam, The Netherlands, 2020; pp. 101–121.
51. Orru, G.; Pettersson-Yeo, W.; Marquand, A.F.; Sartori, G.; Mechelli, A. Using support vector machine to identify imaging biomarkers of neurological and psychiatric disease: A critical review. *Neurosci. Biobehav. Rev.* **2012**, *36*, 1140–1152. [[CrossRef](#)]
52. Genuer, R.; Poggi, J.-M.; Genuer, R.; Poggi, J.-M. *Random Forests*; Springer: Berlin/Heidelberg, Germany, 2020.
53. Hastie, T.; Tibshirani, R.; Friedman, J. The Elements of Statistical Learning: Data Mining, Inference and Prediction. In *Random Forests*; Springer: Berlin/Heidelberg, Germany, 2009; pp. 587–604.
54. Hou, X.; Di, X.; Hou, W.; Wu, L.; Liu, J.; Wang, J.; Su, H.; Lu, X.; Ying, L.; Yu, X. Accuracy evaluation of land use mapping using remote sensing techniques in coastal zone of China. *J. Geo-Inf. Sci.* **2018**, *20*, 1478–1488.
55. Huang, D.; Xu, S.; Sun, J.; Liang, S.; Song, W.; Wang, Z. Accuracy assessment model for classification result of remote sensing image based on spatial sampling. *J. Appl. Remote Sens.* **2017**, *11*, 046023. [[CrossRef](#)]
56. Blanquero, R.; Carrizosa, E.; Ramírez-Cobo, P.; Sillero-Denamiel, M.R. Variable selection for Naïve Bayes classification. *Comput. Oper. Res.* **2021**, *135*, 105456. [[CrossRef](#)]
57. Scholkopf, B.; Smola, A.J. *Learning with Kernels: Support Vector Machines, Regularization, Optimization, and Beyond*; MIT Press: Cambridge, MA, USA, 2018.
58. Hsu, C.-W.; Lin, C.-J. A comparison of methods for multiclass support vector machines. *IEEE Trans. Neural Netw.* **2002**, *13*, 415–425. [[PubMed](#)]
59. Ali, J.; Khan, R.; Ahmad, N.; Maqsood, I. Random forests and decision trees. *Int. J. Comput. Sci. Issues* **2012**, *9*, 272.
60. Liaw, A. Classification and regression by random Forest. *R News* **2002**, 18–22.
61. Belgiu, M.; Drăguț, L. Random forest in remote sensing: A review of applications and future directions. *ISPRS J. Photogramm. Remote Sens.* **2016**, *114*, 24–31. [[CrossRef](#)]
62. Sangeetha, C.; Moond, V.; Rajesh, G.; Damor, J.S.; Pandey, S.K.; Kumar, P.; Singh, B. Remote Sensing and Geographic Information Systems for Precision Agriculture: A Review. *Int. J. Environ. Clim. Chang.* **2024**, *14*, 287–309. [[CrossRef](#)]
63. Burnett, M.W.; White, T.D.; McCauley, D.J.; De Leo, G.A.; Micheli, F. Quantifying coconut palm extent on Pacific islands using spectral and textural analysis of very high resolution imagery. *Int. J. Remote Sens.* **2019**, *40*, 7329–7355. [[CrossRef](#)]
64. Martins, V.S. Deep Learning for Land Cover Classification and Environmental Analysis Using High-Resolution Remote Sensing Data. Ph.D. Thesis, Iowa State University, Ames, IA, USA, 2020.

**Disclaimer/Publisher’s Note:** The statements, opinions and data contained in all publications are solely those of the individual author(s) and contributor(s) and not of MDPI and/or the editor(s). MDPI and/or the editor(s) disclaim responsibility for any injury to people or property resulting from any ideas, methods, instructions or products referred to in the content.